ATLAS NOTE

ATLAS-CONF-2011-095

July 17, 2011

Search for New Physics in Dijet Mass Distributions in 0.81 fb^{-1} of pp Collisions at $\sqrt{s} = 7$ TeV

The ATLAS Collaboration

Abstract

Invariant mass distributions of jet pairs (dijets) produced in LHC proton-proton collisions at a center-of-mass energy $\sqrt{s} = 7$ TeV have been studied with the ATLAS detector using a data set acquired in 2011 with an integrated luminosity of 0.81 fb^{-1}. Dijet masses up to ~ 4.0 TeV are observed in the data, and no evidence of resonance production over background is found. Improved limits have been set at 95% CL for several new physics hypotheses: excited quarks are excluded for masses below 2.91 TeV, axigluons are excluded for masses below 3.21 TeV, and color octet scalar resonances are excluded for masses below 1.91 TeV.

ATLAS-CONF-2011-095
21 July 2011

1 Introduction

The Standard Model (SM) description of high energy proton-proton (pp) collisions is based on the framework of perturbative quantum chromodynamics (QCD), where the most energetic collisions result from the $2 \rightarrow 2$ scattering of a pair of partons (quarks or gluons). Partons emerging from the collision shower and hadronize, in the simplest case producing two jets of particles (a dijet) that may be reconstructed to determine the dijet invariant mass, m_{jj}, the mass of the two-parton system. Dijet mass distributions may be searched for resonances indicating the effects of new phenomena localized near a given mass.

Previous dijet mass distribution studies [1, 2, 3, 4, 5, 6, 7, 8] have shown that this kind of analysis is well suited to early searches at new colliders. Dijet mass distributions may be analyzed to search for resonances indicating new physics, typically using data-driven background estimates that do not rely on detailed QCD calculations.

The present study, in addition to new physics benchmarks used in previous ATLAS dijet analyses, namely excited quarks (q^*) [9, 10], and axigluons [11, 12, 13], makes use of an additional hypothetical object: the color octet scalar (s8) model, one of many possible exotic color resonance models [14]. Any of these would appear as a resonant signal in the vicinity of their intrinsic mass.

The present study is based on pp collisions at a center of mass (CM) energy of 7 TeV produced at the CERN Large Hadron Collider (LHC) and measured by the ATLAS detector, corresponding to an observed integrated luminosity of 0.81 fb^{-1} collected in 2011. The most stringent limits so far from the ATLAS experiment based on dijet mass analysis come from the studies of the 2010 data corresponding to 36 pb^{-1} integrated luminosity [8]. Excited quarks were excluded below 2.15 TeV, quantum black holes below 3.67 TeV, and axigluons below 2.10 TeV.

A detailed description of the ATLAS detector has been published elsewhere [15]. The detector is instrumented over almost the entire solid angle around the pp collision point with layers of tracking detectors, calorimeters, and muon chambers. Jet measurements are made using a finely segmented calorimeter system designed to efficiently detect the high energy jets that are the focus of this study.

The dijet mass, m_{jj}, is derived from the vectorial sum of the four-momenta of the two highest p_{T} jets in the event [1]. The data are binned in m_{jj} choosing bin-widths that are consistent with the detector m_{jj} resolution so that binning effects do not limit the search sensitivity. Since high mass dijets are of greatest interest in these studies, kinematic criteria based on momentum and angular variables are applied to increase the sensitivity to centrally produced high mass resonances.

The angular distribution for $2 \rightarrow 2$ parton scattering is predicted by QCD in the parton CM frame, which moves along the beamline due to the differing momentum fractions (Bjorken x) of the colliding partons. If E is the jet energy and p_z is the z-component of the jet's momentum, the rapidity of the jet is given by $y \equiv \frac{1}{2}\ln(\frac{E+p_z}{E-p_z})$. The rapidities of the two highest p_{T} jets are denoted by y_1 and y_2, and the corresponding rapidity in the parton CM frame is $y^* = \frac{1}{2}(y_1 - y_2)$.

2 Jet reconstruction and event selection

Individual jets are reconstructed using the anti-k_t jet clustering algorithm [16, 17] with the distance parameter $R = 0.6$. The inputs to this algorithm are clusters of calorimeter cells with energy depositions significantly above the measured noise. Jet four-momenta are constructed by the vectorial addition of cell clusters, treating each cluster as an (E, $\vec{p}$) four-vector with zero mass. The jet four-momenta are then corrected for the jet energy scale (JES) as a function of η and p_{T} for various effects, the largest of which are the hadronic shower response and detector material distribution. This is done using a

[1] In the right-handed ATLAS coordinate system, the pseudorapidity η is defined as $\eta \equiv$ -ln tan(θ/2), where the polar angle θ is measured with respect to the LHC beamline. The azimuthal angle ϕ is measured with respect to the x-axis, which points toward the center of the LHC ring. The z-axis is parallel to the anti-clockwise beam viewed from above. Transverse momentum and energy are defined as $p_T = p\sin\theta$ and $E_T = E\sin\theta$, respectively.

calibration scheme based on Monte Carlo (MC) studies including full detector simulation, and validated with extensive test-beam [18] and collision data [19, 20, 21] studies. Measured dijet mass distributions are not unfolded to account for resolution effects.

The current dijet data sample is the result of several stages of event selection, beginning with the hardware trigger. ATLAS has a three-level trigger system, with the first level trigger (L1) being custom-built hardware and the two higher level triggers (HLT) being realized in software. The triggers employed for this study selected events that have at least one large transverse energy deposition, with the transverse energy threshold varying over the period of the data-taking as the instantaneous luminosity of the LHC pp collisions increased.

The m_{jj} distribution is based on the lowest threshold unprescaled jet trigger. Due to the increased LHC instantaneous luminosity, the nominal jet p_{T} threshold for the current data set is 180 GeV, and m_{jj} is required to be greater than 717 GeV to attain full trigger efficiency.

Events are required to have at least one primary collision vertex defined by more than four charged-particle tracks. Events with at least two jets are retained if the next-to-leading jet satisfies $p_{\mathrm{T}}^{j_2} > 30$ GeV. The 30 GeV threshold ensures that reconstruction is fully efficient for both leading jets. Events with a poorly measured jet [22] with p_{T} greater than 30% of the p_{T} of the next-to-leading jet are vetoed to avoid cases where such a jet would cause incorrect identification of the two leading jets (rejecting less than 0.002% of the events).

Finally, events are selected if the two leading jets each satisfy $|\eta_j| < 2.8$ and the rapidity in the parton CM frame satisfies $|y^*| < 0.6$. These criteria favor central collisions and have been shown, based on studies of expected signals and QCD background, to efficiently optimize the signal-to-background in the sample.

3 Comparing data to a smooth background

The observed dijet mass distribution is shown in Fig. 1. The m_{jj} spectrum is fit to the smooth functional form $f(x) = p_1(1-x)^{p_2}x^{p_3+p_4\ln x}$, where $x \equiv m_{jj}/\sqrt{s}$ and the p_i are fit parameters. This ansatz has been shown empirically to accurately model the steeply falling QCD dijet mass spectrum [3, 4, 6, 8]. As noted earlier, the bin widths are consistent with the dijet mass resolution, increasing from ~ 50 to ~ 200 GeV for dijet masses from 0.85 to 4.5 TeV, respectively.

To determine the degree of consistency between the data and the fitted background, the p-value of the fit is calculated using the χ^2 test, determined from pseudoexperiments, as a goodness-of-fit statistic. The resulting p-value is 0.35, indicating that there is no overall disagreement between data and the functional form.

The plot appearing at the bottom of Fig. 1 is the bin-by-bin significance of deviations of data from the prediction. It is formed by calculating p-values in each bin as the first step. These are purely statistical and based on Poisson distributions. In the case of an excess in data in a given bin, the p-value represents the probability to see an excess of that size or larger - vice versa for data being below the prediction. For presentation purposes the p-values are transformed into standard deviations by integration of a Gaussian, and plotted as positive for an excess in data, negative otherwise. Empty bins correspond to insignificant deviations in either direction, with a p-value larger than 0.50, and are therefore not drawn.

4 Searching for resonances

As a more sensitive test of new physics signals, the BUMPHUNTER algorithm [23, 24] is used to establish the presence or absence of a resonance in this spectrum. In the current implementation, the BUMPHUNTER algorithm searches for the signal window with the most significant excess of events above background. Starting with a two-bin window, the algorithm increases the signal window and shifts its location until all possible bin ranges, up to half the mass range spanned by the data, have been tested. The most significant departure from the smooth spectrum ("bump") is defined by the set of bins

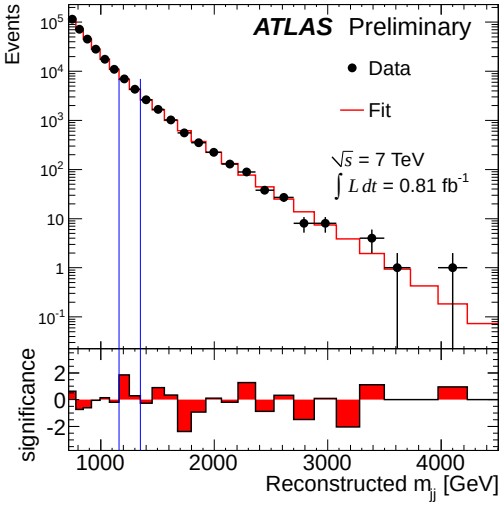

Figure 1: The observed (Data) dijet mass distribution (filled points) fitted using a binned QCD background (Fit) distribution described by the smooth functional form (histogram). The bin-by-bin significance of the data-background difference is shown in the lower panel. Vertical lines show the most significant excess found by the BUMPHUNTER algorithm: the two bins from 1.16 to 1.35 TeV.

that have the smallest probability of arising from a background fluctuation assuming Poisson statistics. The algorithm naturally accounts for the "trials factor" by performing a series of pseudoexperiments to determine the probability that random fluctuations in the background-only hypothesis would create an excess as significant as the observed one anywhere in the spectrum. To improve the background fit before comparison to data, in cases where the χ^2 test on the region with the biggest local excess yields a p-value less than 0.01, this region is excluded, and a new fit is performed. This prevents any potential new physics signal from biasing the background.

In Fig. 1, the most significant discrepancy identified by the BUMPHUNTER algorithm is a 2-bin excess in the dijet mass interval 1.16 to 1.35 TeV. The p-value of observing an excess at least as large as this, assuming a background-only hypothesis in the mass interval considered in this study, is 0.62. Based on this test, we conclude that there is no evidence for a resonance signal in the m_{jj} spectrum.

5 New physics models

To establish exclusion limits and connect to previous studies, three resonant new-physics hypotheses have been simulated. For the first of these, excited quarks, the q^* is assumed to have spin 1/2 and quark-like couplings relative to those of the SM $SU(2)$, $U(1)$, and $SU(3)$ gauge groups, of $f = f' = f_s = 1$, respectively, and a $qg \to q^*$ production model [9, 10] is used. The compositeness scale (Λ) is set to the q^* mass. Signal events are produced using the PYTHIA event generator, a leading-order parton-shower MC generator, with the MRST2007LO* [25] parton distribution functions (PDF's), with settings established by the ATLAS default MC10 [26] Monte Carlo tune. The renormalization and factorization scales are set to the mean p_{T} of the two leading jets. PYTHIA is also used to decay the excited quarks to all possible SM final states, which are predominantly qg, but also qW, qZ, and $q\gamma$. The generated events have been passed through the detailed simulation of the ATLAS detector [27], which uses the GEANT4 package [28] for simulation of particle transport, interactions, and decays. The simulated events are then reconstructed in the same way as the data to produce predicted dijet mass distributions that can be compared with the observed distributions.

The second resonant model is axigluon production [11, 12, 13] via an interaction given by the La-

grangian

$$\mathscr{L}_{Aq\bar{q}} = g_{QCD}\bar{q}A^a_\mu \frac{\lambda^a}{2}\gamma^\mu\gamma_5\, q. \tag{1}$$

where g_{QCD} is the QCD coupling and A^a_μ is the axigluon field representing a massive state with axial coupling to quarks. Parity conservation prevents the axigluon from coupling to two gluons. Parton-level events are generated using the CALCHEP Monte Carlo package [29], for chosen masses of the axigluon. These simulations show that the shape of the axigluon template within the range 0.8 to 1.2 of its peak is very similar to the q^* signal template for all masses of interest. Therefore, the q^* results are employed again in this analysis. CALCHEP is used to supply the theoretical cross section for a given axigluon mass for events within the above range. This narrow-width approximation ignores the non-resonant tails of the axigluon template. Knowing the q^* cross section within the same range, the exclusion limit may be determined, as described in more detail in later sections.

The new resonant hypothesis introduced in the current study, the color octet scalar (s8) model, is a prototype for many possible exotic colored resonances [14]. Color octet resonances can couple to gluons, which have large parton luminosity at the LHC. One possible interaction is

$$\mathscr{L}_{gg8} = g_{QCD}d^{ABC}\frac{\kappa_s}{\Lambda_s}S^A_8F^B_{\mu\nu}F^{C,\mu\nu}\,, \tag{2}$$

where S^A_8 is the color octet scalar field, κ_s is the scalar coupling (assumed to be of order unity), $g^2_{QCD} = 4\pi\alpha_s$ is the QCD coupling associated with the gluon field, and d^{ABC} is the SU(3) isoscalar factor. Λ_s is the new physics scale which is set to the resonance mass, M_{s_8}. This model leads to a very simple event topology, with two gluons in the initial and final states, directly yielding high p_T dijets. MADGRAPH 5 [30] is used to generate parton level events. PYTHIA with CTEQ6L1 PDF's is used in this generation, with the ATLAS MC09' tune [31]. As with the q^* MC samples, these samples have been processed through full ATLAS detector simulation.

The color octet scalar resonance cross section as a function of M_{s_8} given by MADGRAPH is shown in Table 1.

Table 1: Color octet scalar cross sections

M_{s_8} [TeV]	Width [GeV]	σ [pb]
1.0	157.0	83.8
1.3	197.9	12.3
1.5	224.8	3.92
1.7	251.3	1.35
2.0	290.5	0.306
2.5	354.8	0.0324
3.0	417.8	0.447×10^{-2}
3.5	479.9	0.827×10^{-3}
4.0	541.2	0.209×10^{-3}

6 Model dependent limit setting

In the absence of any observed significant discrepancy with the zero-signal hypothesis, the Bayesian method documented in [8] is used to set 95% credibility-level (CL) upper limits. Bayesian credibility intervals are set by defining a posterior probability density from the likelihood function for the observed

mass spectrum, obtained by a fit to the background functional form, and a signal shape derived from MC calculations. A prior probability density constant in all positive values of signal cross section, and zero at negative cross sections, is used. The posterior probability is then integrated to determine the 95% CL for a given range of models, usually parameterized by the mass of the resonance. The Bayesian approach is employed as it simplifies the treatment of systematic uncertainties.

Limits are determined on $\sigma \times \mathscr{A}$, the product of the production cross section and acceptance for a hypothetical new particle decaying into dijets. The acceptance calculation includes all reconstruction steps described above, and assumes that trigger efficiencies are near 100%.

The effects of systematic uncertainties due to the luminosity and the JES have been included in this analysis. The effect of the jet energy resolution (JER) uncertainty is found to be negligible. The luminosity uncertainty for 2011 data is 4.5%, based on the 2010 luminosity calibration [32] which has been updated for 2011 data by using the ATLAS forward and scintillating tile calorimeters. The systematic uncertainty on the JES was taken from 2010 data [33] analysis, and has been adapted to the 2011 analysis taking into account in particular the new event pileup conditions (described below). The background parameterization uncertainty is handled as described in [8], taking the uncertainties from the background fit results. These uncertainties are incorporated into the analysis by varying all sources according to Gaussian probability distributions and convolving them with the Bayesian posterior probability distribution. Credibility intervals are then calculated numerically from the resulting convolutions.

In 2011, the instantaneous luminosity has risen to a level where detailed corrections must be made for events whose presence affects the measurement of calorimeter energy depositions associated with the hard-scattering event under study, referred to collectively as "pileup". All MC samples have included a Poisson distributed number of MC minimum bias events added to the hard interaction to account for "in-time" pileup caused by additional events in the same bunch crossing. Further account must be taken of "out-of-time" pileup originating from events in bunches preceding or following the one of interest in combination with the long response time of the liquid Argon calorimeters. With the 50 ns bunch spacing in the LHC for these data, up to 12 preceding bunches and 1-2 following bunches contribute to out-of-time pileup. While conditions modelled in MC are realistic, they do not perfectly match data due to bunch train structure and instantaneous luminosity variations in the LHC. To remedy this, the MC events are reweighted to remove these residual differences compared to data. Following this procedure the pileup description in MC is sufficiently good that no additional uncertainty on the JES is required for jets with $p_{\mathrm{T}} > 100$ GeV.

The results of the Bayesian limit setting are shown in Fig. 2. Fig. 2(a) shows the results for excited quarks and axigluons, using the same analyses as were applied to 2010 data. For q^* the expected mass limit at 95% CL is 2.77 TeV, and the observed limit is 2.91 TeV.

As in 2010, the axigluon results are based on the q^* $\sigma \times \mathscr{A}$ limit curves using the methods described in detail in Section VII. The q^* acceptance, $\mathscr{A}$, ranges from 37 to 51% for m_{q^*} from 0.8 to 5.0 TeV, respectively, due to selection criteria; and is never lower than 47% above 1.1 TeV. The loss of acceptance comes mainly from the rapidity requirements, which ensure that the candidate events have a high signal-to-background ratio. The expected axigluon mass limit at 95% CL is 3.02 TeV, and the observed limit is 3.21 TeV.

Fig. 2(b) shows the $\sigma \times \mathscr{A}$ limit setting for color octet resonances, performed here for the first time in ATLAS. As in the q^* analysis, this study is based on fully simulated MC samples. The expected mass limit at 95% CL is 1.71 TeV, and the observed limit is 1.91 TeV. Since the color octet scalar cross section decreases rapidly with m_{jj} these limits are considerably lower than those for excited quarks and axigluons.

For all three models used in the current study, if systematic uncertainties had not been included the exclusion limits would be about 60 GeV higher.

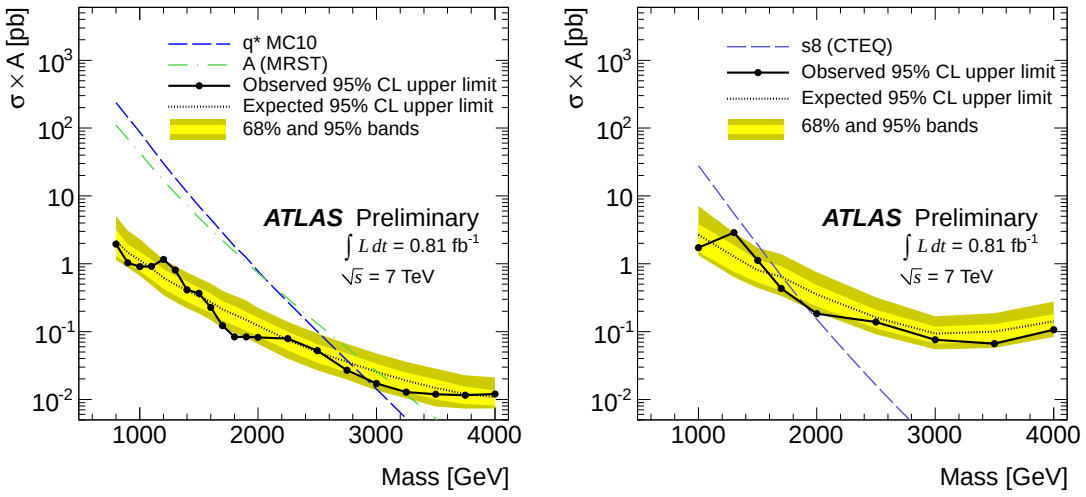

(a) Excited-quark and axigluon models.

(b) Color octet scalar model.

Figure 2: Limit setting using $\sigma \times \mathscr{A}$ theory curves for (a) excited quarks (blue dashed) and axigluons (green dot-dashed), and (b) color octet scalar resonances (blue dashed). Black filled circles are the 95% CL upper limit from data for $\sigma \times \mathscr{A}$ as a function of m_{jj}. The black dotted curve shows the 95% CL upper limit expected from Monte Carlo and the light and dark yellow shaded bands represent the 68% and 95% contours of the expected limit, respectively. For a given new physics model, the observed (expected) limit occurs at the crossing of its $\sigma \times \mathscr{A}$ curve with the observed (expected) 95% CL upper limit curve.

7 Model independent limit setting

A final resonance analysis has been applied to the current data set: the more model-independent signal template used previously [8], which is a Gaussian profile with means ranging from 0.9 to 4.0 TeV and with the width, σ, varying from 5% to 15% of the mean.

As in model dependent limit setting, systematic uncertainties are treated using pseudoexperiments to marginalize the posterior probabilities that depend on parameters subject to systematic uncertainty. Given that the decay of the dijet final state has not been modelled, assuming only that the resulting dijet width is Gaussian in shape, the treatment of the JES is adjusted by modelling it as an uncertainty of at most 4% in the central value of the Gaussian signal.

The results of $\sigma \times \mathscr{A}$ limit setting for the Gaussian template model are shown in Fig. 3. These limits may be utilized for another new physics model with the following procedure: (1) Compute the acceptance $\mathscr{A}$ using a standard MC calculation while applying the jet p_{T} and y requirements used in the current analysis to determine the expected signal shape in m_{jj}. (2) Since a Gaussian signal shape has been assumed in determining the limits, any long tails in m_{jj} should be removed. The recommendation is to retain events with m_{jj} between 0.8 and 1.2 times the simulated mass. Determine the mean mass, m, and the width, σ_m of this truncated signal. (3) The fraction of MC events surviving these first two procedures is the estimate of the modified acceptance, $\mathscr{A}_{mod}$. (4) From Fig. 3, or a corresponding table, use m to pick the nearest mass point, rounding down to be conservative. (5) For this mass point, pick a Gaussian width $\sigma_{Gaussian}/m_{Gaussian}$ that is well contained in the truncated mass range. For m_{q^*} a good choice was σ_m = (1.2m-0.8m)/5 so that 95% of the Gaussian spans $4 \times \frac{0.4m}{5}$. Use this value to pick the closest $\sigma_{Gaussian}/m_{Gaussian}$ curve, rounded up to be conservative. (6) The chosen value is the 95% CL upper limit in pb, corresponding to accepted events. Using the theoretical cross section given by the model, compare this to $\sigma_{Theory} \times BR \times \mathscr{A}_{mod}$.

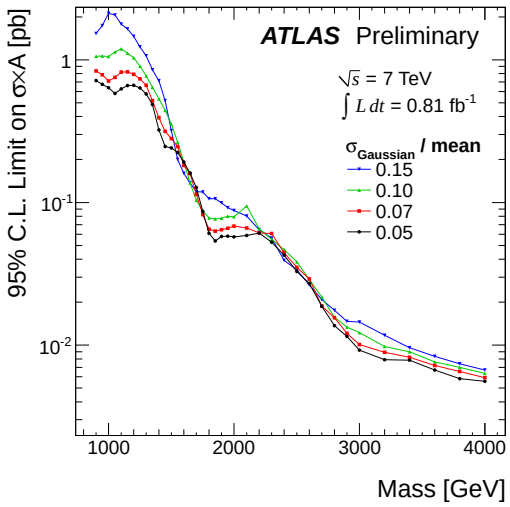

Figure 3: The 95% CL upper limits on $\sigma \times \mathscr{A}$ for a simple Gaussian resonance decaying to dijets as a function of the mean mass, m, for four values of $\sigma_{Gaussian}/m$, taking into account both statistical and systematic uncertainties.

This procedure works because most resonances are approximately Gaussian near the core, and the tails are buried under background. It also may be applied to parton-level simulations because tests have established that uncertainties due to detector resolution are smaller than those associated with this limit setting method.

8 Conclusion

The dijet mass distribution has been measured by the ATLAS experiment spanning dijet masses up to ≈ 4.0 TeV using 0.81 fb^{-1} of 7 TeV pp collision data taken in 2011. It is in good agreement with a smooth function as expected from the SM, and there is no evidence for resonance production. Therefore, stringent 95% CL mass limits have been determined, as summarized in Table 2. As in previous studies, all limits are set using Bayesian methodology, and systematic uncertainties are included in the analysis. For excited quarks and axigluons, the current results exceed the limits obtained with the 2010 data by approximately one TeV. Exclusion limits on color octet scalar resonances have been established for the first time in ATLAS.

Table 2: The 95% CL mass lower limits for the models examined in this study. All limit analyses are Bayesian, and include systematic uncertainties.

Model	95% CL Limits (TeV)	
	Expected	Observed
Excited Quark q^*	2.77	2.91
Axigluon	3.02	3.21
Color Octet Scalar	1.71	1.91

References

[1] UA1 Collaboration, G. Arnison et al., *Angular distributions and structure functions from two-jet events at the CERN SPS pbar-p collider*, Phys. Lett. B **136** (1984) 294.

[2] UA2 Collaboration, P. Bagnaia et al., *Measurement of jet production properties at the CERN Collider*, Phys. Lett. B **144** (1984) no. 3-4, 283–290.

[3] CDF Collaboration, T. Aaltonen et al., *Search for New Particles Decaying into Dijets in $p\bar{p}$ Collisions at $\sqrt{s} = 1.96$ TeV*, Phys. Rev. D **79** (Aug, 2009) 112002, arXiv:0812.4036 [hep-ex].

[4] ATLAS Collaboration, *Search for New Particles in Two-Jet Final States in 7 TeV Proton-Proton Collisions with the ATLAS Detector at the LHC*, Phys. Rev. Lett. **105** (2010) 161801, arXiv:1008.2461 [hep-ex].

[5] ATLAS Collaboration, *Search for Quark Contact Interactions in Dijet Angular Distributions in pp Collisions at sqrt(s) = 7 TeV Measured with the ATLAS Detector*, Phys. Lett. B **694** (2011) 327, arXiv:1009.5069 [hep-ex].

[6] CMS Collaboration, *Search for Dijet Resonances in 7 TeV pp Collisions at CMS*, Phys. Rev. Lett. **105** (Nov, 2010) 211801.

[7] CMS Collaboration, *Measurement of Dijet Angular Distributions and Search for Quark Compositeness in pp Collisions at $\sqrt{s} = 7$ TeV*, Phys. Rev. Lett. **106** (2011) 201804, arXiv:1102.2020 [hep-ex].

[8] ATLAS Collaboration, *Search for New Physics in Dijet Mass and Angular Distributions in pp Collisions at $\sqrt{s}$ = 7 TeV Measured with the ATLAS Detector*, New Journal of Physics **13** (2011) 053044, arXiv:1103.3864 [hep-ex].

[9] U. Baur, I. Hinchliffe, and D. Zeppenfeld, *Excited Quark Production at Hadron Colliders*, Int. J. Mod. Phys. **A2** (1987) 1285.

[10] U. Baur, M. Spira, and P. M. Zerwas, *Excited Quark and Lepton Production at Hadron Colliders*, Phys. Rev. **D42** (1990) 815–824.

[11] P. Frampton and S. Glashow, *Chiral Color: An Alternative to the Standard Model*, Phys. Lett. B **190** (1987) 157.

[12] P. Frampton and S. Glashow, *Unifiable Chiral Color With Natural Gim Mechanism*, Phys. Rev. Lett. **58** (1987) 2168.

[13] J. Bagger, C. Schmidt, and S. King, *Axigluon Production In Hadronic Collisions*, Phys. Rev. D **37** (1988) 1188.

[14] T. Han, I. Lewis, and Z. Liu, *Colored Resonant Signals at the LHC: Largest Rate and Simplest Topology*, JHEP **12** (2010) 085, arXiv:1010.4309 [hep-ph].

[15] ATLAS Collaboration, *The ATLAS Experiment at the CERN Large Hadron Collider*, JINST **3** (2008) S08003.

[16] M. Cacciari, G. Salam, and G. Soyez, *The anti-k_T jet clustering algorithm*, JHEP **04** (2008) 063, arXiv:hep-ph/0802.1189.

[17] M. Cacciari and G. P. Salam, *Dispelling the N^3 Myth*, Phys. Lett. **B641** (2006) 57, arXiv:hep-ph/0512210.

[18] P. Adragna et al., *Measurement of pion and proton response and longitudinal shower profiles up to 20 nuclear interaction lengths with the ATLAS tile calorimeter*, Nucl. Instrum. Meth. **A615** (2010) 158–181.

[19] ATLAS Collaboration, *ATLAS Calorimeter Response to Single Isolated Hadrons and Estimation of the Calorimeter Jet Scale Uncertainty*, ATLAS-CONF-2010-052 (2010) .

[20] ATLAS Collaboration, *Jet energy scale and its systematic uncertainty in ATLAS for jets produced in proton-proton collisions at $\sqrt{s} = 7$ TeV*, ATLAS-CONF-2010-056 (2010) .

[21] ATLAS Collaboration, *Update on the Jet Energy Scale Systematic Uncertainty for Jets Produced in Proton-Proton Collisions at $\sqrt{s} = 7$ TeV Measured with the ATLAS detector*, ATLAS-CONF-2011-007 (2011) .

[22] ATLAS Collaboration, *Data-Quality Requirements and Event Cleaning for Jets and Missing Transverse Energy Reconstruction with the ATLAS Detector in Proton-Proton Collisions at a Center-of-Mass Energy of $\sqrt{s} = 7$ TeV*, ATLAS-CONF-2010-038 (2010) .

[23] CDF Collaboration, T. Aaltonen et al., *Global Search for New Physics with 2.0 fb^{-1} at CDF*, Phys. Rev. **D79** (2009) 011101, `arXiv:0809.3781 [hep-ex]`.

[24] G. Choudalakis, *On Hypothesis Testing, Trials Factor, Hypertests and the BumpHunter*, `arXiv:1101.0390 [physics.data-an]`.

[25] A. Sherstnev and R. S. Thorne, *Parton Distributions for LO Generators*, Eur. Phys. J. **C55** (2008) 553, `arXiv:0711.2473 [hep-ph]`.

[26] ATLAS Collaboration, *AMBT1 tune of Pythia to Minimum Bias results*, ATL-CONF-2010-031 .

[27] ATLAS Collaboration, *The ATLAS Simulation Infrastructure*, Eur. Phys. J **C70** (2010) 823, `arXiv:1005.4568v1 [physics.ins-det]`.

[28] GEANT4 Collaboration, S. Agostinelli et al., *GEANT4: A simulation toolkit*, Nucl. Instrum. Meth. **A506** (2003) 250–303.

[29] A. Pukhov, *CalcHEP 3.2: MSSM, Structure Functions, Event Generation, Batchs, and Generation of Matrix Elements for Other Packages*, `arXiv:hep-ph/0412191`.

[30] J. Alwall, M. Herquet, F. Maltoni, O. Mattelaer, and T. Stelzer, *MadGraph 5 : Going Beyond*, `arXiv:1106.0522 [hep-ph]`.

[31] ATLAS Collaboration, *ATLAS Monte Carlo Tunes for MC09*, ATL-PHYS-PUB-2010-002 (2010) .

[32] ATLAS Collaboration, *Updated Luminosity Determination in pp Collisions at $\sqrt{s} = 7$ TeV using the ATLAS Detector*, ATLAS-CONF-2011-011 (2011) .

[33] ATLAS Collaboration, *Jet energy scale and its systematic uncertainty in proton-proton collisions at $\sqrt{s} = 7$ TeV in ATLAS 2010 data*, ATLAS-CONF-2011-032 (2011) .

Appendix: Additional Material

Trigger studies have been done to establish the 99% efficiency point for all triggers used in the current analysis. One example is Fig. 4, the efficiency plot for the j180 jet trigger.

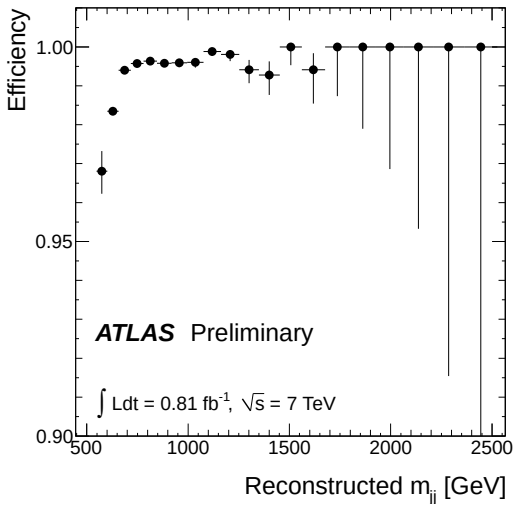

Figure 4: Efficiency of the EF j180 trigger as a function of m_{jj}.

A correction has been implemented for a read-out defect in the liquid-argon calorimetry. In a significant part of current 2011 data, a hardware problem caused part of the electromagnetic barrel calorimeter to not be read out. Studies of the JetETmiss Performance group identify the region where jets are significantly impacted as: ϕ from -0.88 to -0.5 and η from -0.1 to 1.5. Affected jets have been found on average to lose 20-30% of their energy, as well as to suffer from deterioration of the jet energy and angular resolution. Official recommendations are applied, which are for the moment to treat jets as "ugly" if they fall within the above region. In the dijet analysis ugly jets cause an event to be rejected if they have more than 30% of the p_{T} of the next-to-leading jet. This leads to a loss of statistics on the order of 0.002%.

Excited quark resonances due to new phenomena would appear as bumps above the QCD background. For illustration, Fig. 5 shows excited quark mass templates superimposed on the m_{jj} distribution in the current data set. BUMPHUNTER analysis of the m_{jj} distribution in the current data set shows that the most discrepant interval is from 1162 to 1350 GeV. The p-value associated with this fluctuation is 0.62, consistent with QCD.

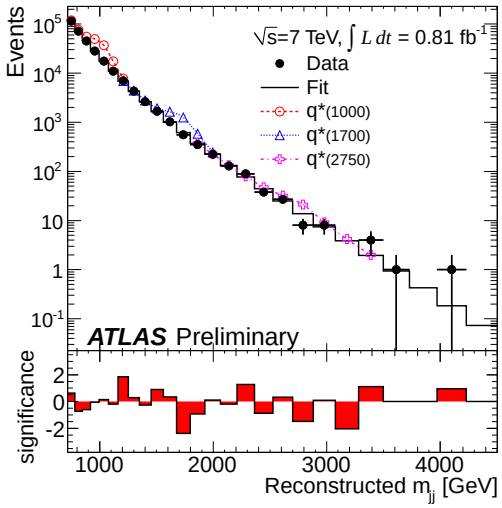

Figure 5: The observed (Data) dijet mass distribution (filled points) fitted using a binned QCD background (Fit) distribution described by the smooth functional form (histogram). The bin-by-bin significance of the data-background difference is shown in the lower panel. For illustration, excited quark mass templates have been superimposed on the data.

Fig. 6(a), the BUMPHUNTER tomography plot, shows the significance of each mass interval. Each red line corresponds to a mass interval (x-axis). The y-axis position of each line corresponds to the Poisson p-value of seeing as many data as were seen in that mass interval, given the expected number of events in the same interval. The BUMPHUNTER tries all intervals, from narrow to wide, and in the end it keeps the one at the bottom, which is the most unlikely to be just a statistical fluctuation. From the above tomography we conclude that there is no other region competing with the most discrepant one.

Fig. 6(b) shows the likelihood analysis used to determine the p-value for the most discrepant interval in the m_{jj} distribution.

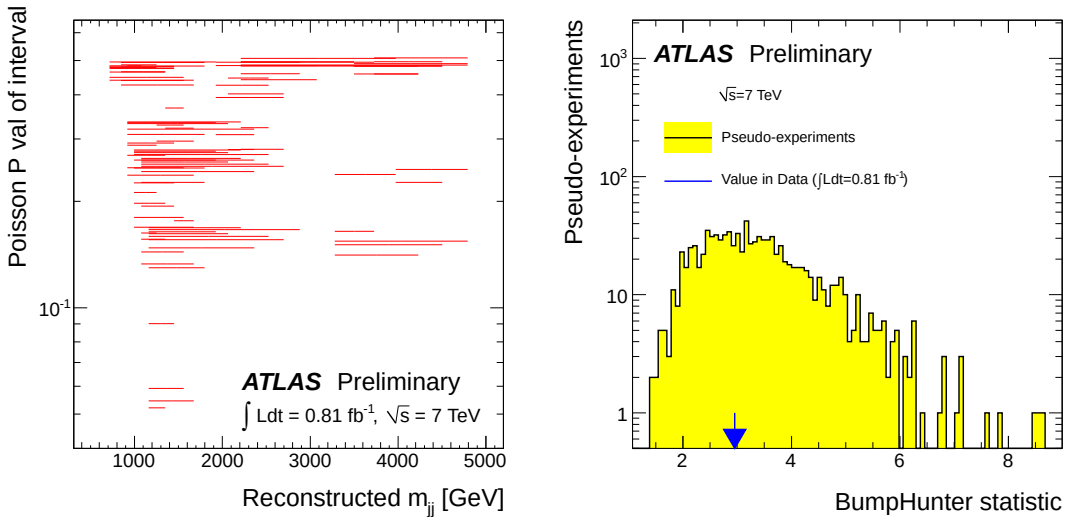

(a) BUMPHUNTER scan tomography of the m_{jj} distribution.

(b) Likelihood analysis used to calculate the p-value in the interval of interest in the m_{jj} distribution.

Figure 6: BUMPHUNTER analysis

Gaussian signal templates have been used to set model-independent limits on $\sigma \times \mathscr{A}$ in the current data. The 95% CL limits shown in Fig. 3 are listed in Table 3, as a function of dijet resonance mass expressed in terms of σ/m after all event selection criteria have been applied. The variation in these limits as a function of mass and width reflects the statistical fluctuations of data in the binned m_{jj} distribution used to set them.

Table 3: The 95% CL upper limit on $\sigma \times \mathscr{A}$ [pb] for the Gaussian model. The symbols m_G and σ_G are, respectively, the mean mass and RMS width of the Gaussian.

m_G	σ_G/m_G			
(GeV)	5%	7%	10%	15%
900	0.73	0.85	1.1	1.6
950	0.69	0.80	1.1	1.8
1000	0.65	0.72	1.1	2.2
1050	0.59	0.77	1.2	2.1
1100	0.64	0.83	1.2	1.8
1150	0.67	0.84	1.1	1.7
1200	0.67	0.81	1.1	1.5
1250	0.65	0.75	0.92	1.3
1300	0.59	0.68	0.79	1.1
1350	0.49	0.53	0.66	0.87
1400	0.33	0.40	0.54	0.73
1450	0.25	0.32	0.45	0.53
1500	0.25	0.29	0.36	0.32
1550	0.23	0.25	0.27	0.20
1600	0.20	0.19	0.20	0.16
1650	0.16	0.16	0.14	0.14
1700	0.13	0.12	0.11	0.12
1750	0.088	0.084	0.089	0.12
1800	0.062	0.066	0.079	0.11
1850	0.055	0.064	0.078	0.11
1900	0.059	0.066	0.079	0.10
1950	0.059	0.067	0.081	0.094
2000	0.058	0.070	0.081	0.089
2100	0.060	0.067	0.096	0.082
2200	0.062	0.062	0.067	0.066
2300	0.054	0.062	0.056	0.057
2400	0.044	0.045	0.048	0.040
2500	0.033	0.036	0.039	0.034
2600	0.028	0.030	0.029	0.027
2700	0.019	0.019	0.022	0.021
2800	0.014	0.016	0.016	0.018
2900	0.012	0.012	0.014	0.015
3000	0.009	0.010	0.012	0.015
3200	0.008	0.009	0.010	0.012
3400	0.008	0.008	0.009	0.010
3600	0.007	0.007	0.008	0.009
3800	0.006	0.007	0.007	0.008
4000	0.006	0.006	0.006	0.007